ORIGINAL PAPER



Grain growth inhibited during grain size-sensitive creep in polycrystalline ice: an energy dissipation-rate perspective

Tess E. Caswell^{1,2} • Reid F. Cooper¹

Received: 7 February 2022 / Accepted: 23 May 2022 / Published online: 2 July 2022 © The Author(s), under exclusive licence to Springer-Verlag GmbH Germany, part of Springer Nature 2022

Abstract

Experiments in which two identical polycrystalline ice Ih specimens are simultaneously subjected to the same time–temperature history while one of the specimens is actively deformed via grain size-sensitive (GSS) creep demonstrate distinctly different microstructural evolution: for particular ranges of starting grain size and differential stress, grains do not grow in the deforming specimen. Ice Ih specimens having initial, uniform grain sizes in the range $d=6-63~\mu m$ were tested in pairs that were subjected to identical time–temperature conditions (durations $t=4-12~{\rm days}$; $T=240~{\rm K}$) but of which only one was subjected to differential stress ($\sigma_1=0.25-1.85~{\rm MPa}$; $\sigma_3=0$). Comparing specimens within a pair, for those with coarser initial grain size, the deformed specimens exhibit suppressed or no grain growth. Our results are interpreted from the perspective of nonequilibrium thermodynamics, specifically comparing the energy dissipation rates associated with both grain growth and plastic flow: if the rate of energy dissipation associated with flow exceeds that of grain growth, the grains will not grow. An examination of the limited database on GSS flow and grain growth in silicates conforms to our analysis. The results are applied to the question of the mechanical evolution of terrestrial glaciers and to the ice-rich shells of the outer satellites.

Keywords Normal grain growth · Grain size-sensitive plasticity · Energy dissipation · Ice · Rheology

Introduction

Grain size evolution in deforming, polycrystalline ice is critical to processes both on and off the Earth. Terrestrially, grain size impacts rheology and affects the rate of sea-level rise through the rate of ice loss from the Greenland and Antarctic Ice Sheets. Although both field data and numerical models suggest that ice sheets are susceptible to catastrophic collapse on timescales less than 10³ a (Pollard and DeConto 2009; Sejrup et al. 2016), the response of these ice sheets to climatic forcing remains one of the greatest uncertainties in projections of twenty-first-century sea-level rise (Alley and Joughin 2012; Willis and Church 2012). Models of ice sheet stability incorporate factors including climate coupling

☑ Reid F. Cooper reid_cooper@brown.eduTess E. Caswell

tess.e.caswell@gmail.com

Department of Earth, Environmental and Planetary Sciences, Brown University, Providence, RI 02912, USA

Present Address: KBR, Incorporated, Houston, TX 77058, USA (Gasson et al. 2016), grounding line dynamics and buttressing by floating ice shelves (Pollard and DeConto 2009), basal hydrology (Schoof 2010), and ice rheology (Deblonde and Peltier 1991; Pettit et al. 2011), but the latter factor is complicated by the observed grain size sensitivity of polycrystalline ice at conditions appropriate to glaciers and ice sheets (Cuffey et al. 2000; Goldsby and Kohlstedt 2001; Stern et al. 1997). An additional element—grain size—must therefore be added to ice-sheet flow models, and accurately predicting ice sheet stability in the face of a warming climate thus requires knowledge of grain size evolution within deforming ice.

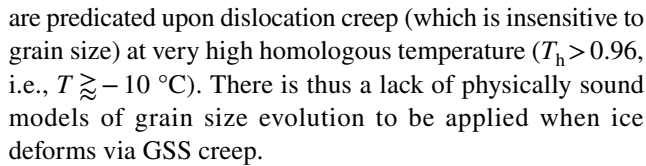
Beyond Earth, polycrystalline ice flows within the interiors of icy moons of the outer solar system. Jupiter's moon Europa, for example, possesses an ice I shell up to 30 km thick overlying a liquid water-rich ocean (Billings and Kattenhorn 2005; Nimmo et al. 2003; Ojakangas and Stevenson 1989). The shell experiences convection, driving tectonic features observed on the moon's surface (Kattenhorn and Prockter 2014; Pappalardo et al. 1998). The vigor of convection and, hence, an understanding of the driving stresses for tectonic deformation are a strong function of the viscosity of the ice (Collins et al. 2009). Europa's ice



shell is simultaneously heated by tidal dissipation, which depends upon the viscosity of the ice (Tobie et al. 2003) and upon convective stresses if present (McCarthy and Cooper 2016). At Saturn, the icy moon Enceladus erupts plumes of water vapor and ice from over one hundred active vents along four strike-slip faults known as "Tiger Stripes" in the moon's South Polar Terrain (Porco et al. 2006, 2014). Plume activity is regulated by tidal forces (Porco et al. 2014) and is thought to be the source of Saturn's E-ring (Baum et al. 1981; Kempf et al. 2010; Spahn et al. 2006), suggesting that the geysers have persisted for some time. The relationships between tidal heating, possible convection beneath the South Polar Terrain, and deformation in the vicinity of the "Tiger Stripes" depend strongly on the local viscosity structure of the ice shell. Because grain size-sensitive (GSS) rheology is expected to dominate at the pressures and temperatures within these deforming ice I shells (Barr and Pappalardo 2005; Barr and Showman 2009), the evolution of grain size in the course of any inelastic material response such as convection is a critical physical process that should be represented in any authoritative model of icy satellite geophysics.

Modeling grain size evolution in a deforming, polycrystalline material generally involves the application of piezometers, which are semi-empirical formulae describing the relationship between deviatoric stress and the grain size set by dynamic recrystallization (Twiss 1977; Poirier 1985, p. 179; Shimizu 1998). A second approach, similar to piezometers, is the "paleowattmeter" which describes recrystallized grain size as a function of the relative energy dissipation rate by each rheological mechanism effecting creep (Austin and Evans 2007). While these relationships can be applied to in-situ and ice core measurements in terrestrial, glaciological applications, logistical challenges have so far prevented direct observation of microstructures in some of the most dynamic glaciological settings, such as the margins of ice streams. It is also, of course, not yet possible to measure the grain size within the shell of an icy satellite (although grain size evolution of frost deposited on the surfaces of the satellites can be inferred from spectral observations (Clark 1981) and has been modeled (Clark et al. 1983)). Thus, the grain size in these dynamic regions remains relatively unconstrained.

Previous authors have adapted standard piezometric relationships to predict the grain size in ice deforming at a steady state (Montagnat and Duval 2000; Barr and McKinnon 2007; Behn et al. 2021; Ranganathan et al. 2021). Of particular relevance to this study is the model of Barr and McKinnon (2007), which determined the equilibrium grain size in a convecting ice shell deforming via GSS creep. The model, however, assumed that dynamic recrystallization occurs during GSS creep in ice, which recent experimental work has shown to be inappropriate (Caswell et al. 2015). Other models, such as that of Montagnat and Duval (2000),



We propose—and, in this experimental study, demonstrate—that a comprehensive model of grain size evolution should consider the rates of (free) energy dissipation. When sustained differential stress (nonequilibrium mechanical potential) is applied to a system—as in, e.g., a creep test on a specimen of polycrystalline ice or, naturally, when convective stress affects a planetary ice shell—the system texture evolves to a non-equilibrium steady-state whereby the additional energy input is dissipated by the most rapid means available. This postulate is an application of the maximum entropy-production principle in dynamics, i.e., non-equilibrium thermodynamics, to crystalline plasticity (e.g., Kondepudi and Prigogine 1998, Ch. 15). In the physics probed here, two physical processes of energy dissipation compete: grain growth and GSS rheology. In general, grains grow because the free-energy density associated with grain boundaries is thereby lowered; the rate of grain growth diminishes with growth because the driving potential is reduced. Strain energy density associated with a persistent, unvarying deviatoric stress is dissipated by inelastic flow, and for grain-size-sensitive rheology, the rate of that dissipation is diminishes as grains grow. The criterion that a system evolves to a texture that, at a steady state, maintains as high an energy dissipation rate as practicable means that the response overall is dominated by the competing mechanism that dissipates energy most rapidly. Calculating relative energy dissipation rates of processes occurring at grain boundaries in a polycrystalline material deforming via GSS creep reveals that, for certain conditions of stress and grain size, the system can dissipate energy faster via GSS creep than by grain growth. Under such conditions, grain growth would be suppressed.

Theoretical considerations

Normal grain growth is driven by the chemical potential difference across a curved grain boundary (Feltham 1957; Hillert 1965; Sutton and Balluffi 1995, p. 524; Alley et al. 1995). That difference is defined by:

$$\Delta\mu_{GG} = \frac{\zeta\gamma_{GB}\Omega}{\Delta r},\tag{1}$$

where μ is the chemical potential with subscript GG representing grain growth, ζ is a constant depending on the grain-growth model, γ_{GB} is grain boundary (or solid–solid interfacial) energy per unit area, Ω is molecular volume and



r is grain radius. The value of γ_{GB}^{ice-I} for high-angle (>15°) tilt boundaries in ice has been measured as 0.065 J m⁻², although this value varies as a function of grain boundary misorientation (Druetta et al. 2014; cf. Ketcham and Hobbs 1969; Sutton and Balluffi 1995, Ch. 2). This chemical potential difference effects the diffusion of atoms/molecules across a grain boundary from the more tightly curved grain (Hillert 1965; Alley et al. 1995; Sutton and Balluffi 1995, p. 524). A grain with a larger radius of curvature will thus "eat" a neighboring grain with a smaller radius of curvature.

When a deviatoric stress is applied to the aggregate, an additional difference in chemical potential can be characterized at the scale of the grain size. Normal tractions on grain boundaries vary as a function of boundary orientation relative to the applied stress tensor. The spatial difference in tractions drives the chemical diffusion of atoms/ions from boundaries of relatively high traction to those of relatively low traction (Nabarro 1948; Herring 1950; Coble 1963; Raj and Ashby 1971). These are the physics of diffusion creep and, in part, of grain boundary sliding (GBS; cf. Goldsby and Kohlstedt (1997)). The chemical potential difference associated with spatial variations of normal traction (subscript *Tr*) on the grain boundary is expressed by (Herring 1950; Raj 1975):

$$\Delta \mu_{Tr} = \Delta T_n \Omega, \tag{2}$$

where T_n is the normal traction (units of stress) at a point along the boundary. For a faceted grain boundary deforming via steady-state grain boundary sliding (as is the case for polycrystalline ice at planetary conditions (e.g., Barr and Pappalardo 2005; cf. Hondoh and Higashi 1978; Goldsby and Kohlstedt 2001)), the normal traction at the center of a facet may be more than twice that at its edges (Raj 1975).

The two chemical potential differences are illustrated in Fig. 1a for the situation under consideration, i.e., a polycrystalline material subjected to persistent deviatoric stress. Both grain growth and grain size-sensitive creep are facilitated by chemical diffusion: for grain growth, all ionic species in a compound must diffuse across a grain boundary, and for GSS creep, ionic species must diffuse along a grain boundary and/or through the crystal lattice. From the perspective of nonequilibrium thermodynamics, however, the critical issue is not the relative size of the potential energy differences that dictate the dominant kinetic response, but rather the relative steepness of the potential gradients, which, ceteris paribus, characterize the dynamics: if the rate of reduction of chemical potential overall is greater via GSS flow than by grain growth, then growth will be suppressed. One can therefore predict which mechanism dominates overall kinetics by calculating the rates of bulk energy dissipation for each process and comparing them.

The macroscopic manifestation of Eq. (1) is normal grain growth as a function of time, expressed by

$$d^2 - d_o^2 = 4Kt, (3)$$

where d is final grain size (grain diameter), d_o is initial grain size, t is time, and K is the kinetic growth-rate constant, which is temperature-sensitive following Boltzmann's statistics, i.e., $K = K_o \exp(-Q_{gr}/RT)$, where Q_{gr} is the activation enthalpy for the growth process and RT has the usual meaning (Arena et al. 1997; cf. Gow 1969; Poirier 1985, p. 72; Azuma et al. 2012). The pre-exponential constant K_o incorporates the normalized (to RT) driving potential (e.g., Schmalzried 1995, p. 145). Equation (3) can be inserted into a simple geometrical expression to formulate the time-dependent total grain boundary energy per unit volume during grain growth:

$$E_{GG} = \frac{E_{GB}}{V} = \frac{6\gamma_{GB}}{\sqrt{d_o^2 + 4Kt}},$$
 (4)

where E_{GB} = (#grains × grain surface area × γ_{GB}), V is volume and, thus, E_{GG} has units J m⁻³. The number of grains is estimated by dividing a unit volume by the grain volume, and the constant in Eq. (4) arises from the surface area to volume ratio of the grains. In that no work is accomplished in grain growth, E_{GG} is dissipated energy. Equation (4) can then be differentiated with respect to time to produce the energy dissipation rate associated with grain growth:

$$\dot{E}_{GG} = -12\gamma_{GB}K(d_o^2 + 4Kt)^{-3/2}. (5)$$

There is, likewise, no work accomplished in plastic deformation: it is all dissipation of stored elastic strain energy. In general, the rate of this dissipation is characterized by (for steady-state flow):

$$\dot{E}_{Pl} = \sigma \dot{\varepsilon}_{Pl},\tag{6}$$

where σ is (deviatoric) stress and $\dot{\varepsilon}_{Pl}$ is steady-state strain rate (the Pl subscript signifying plasticity). Rate-sensitive plasticity in polycrystalline ice incorporates four kinetically independent mechanisms (cf. Goldsby and Kohlstedt 2001): (i) diffusion creep (which is rate-limited by chemical diffusion of H^+ , O^{2-} or, potentially, H_2O molecules either through the lattice or along grain boundaries), (ii) grain boundary sliding (GBS; this mechanism involves serial, i.e., dependent, kinetic steps of (a) sliding along the grain boundary via the motion of boundary-defining point and line defects and (b) lattice dislocation glide on the basal (0001) plane [cf. Liu et al. 1993)], (iii) dislocation creep (which is rate-limited by the glide and climb/cross-slip of lattice dislocations on multiple slip systems within ice grains) and (iv) rate-independent dislocation glide (i.e., yielding, in the engineering



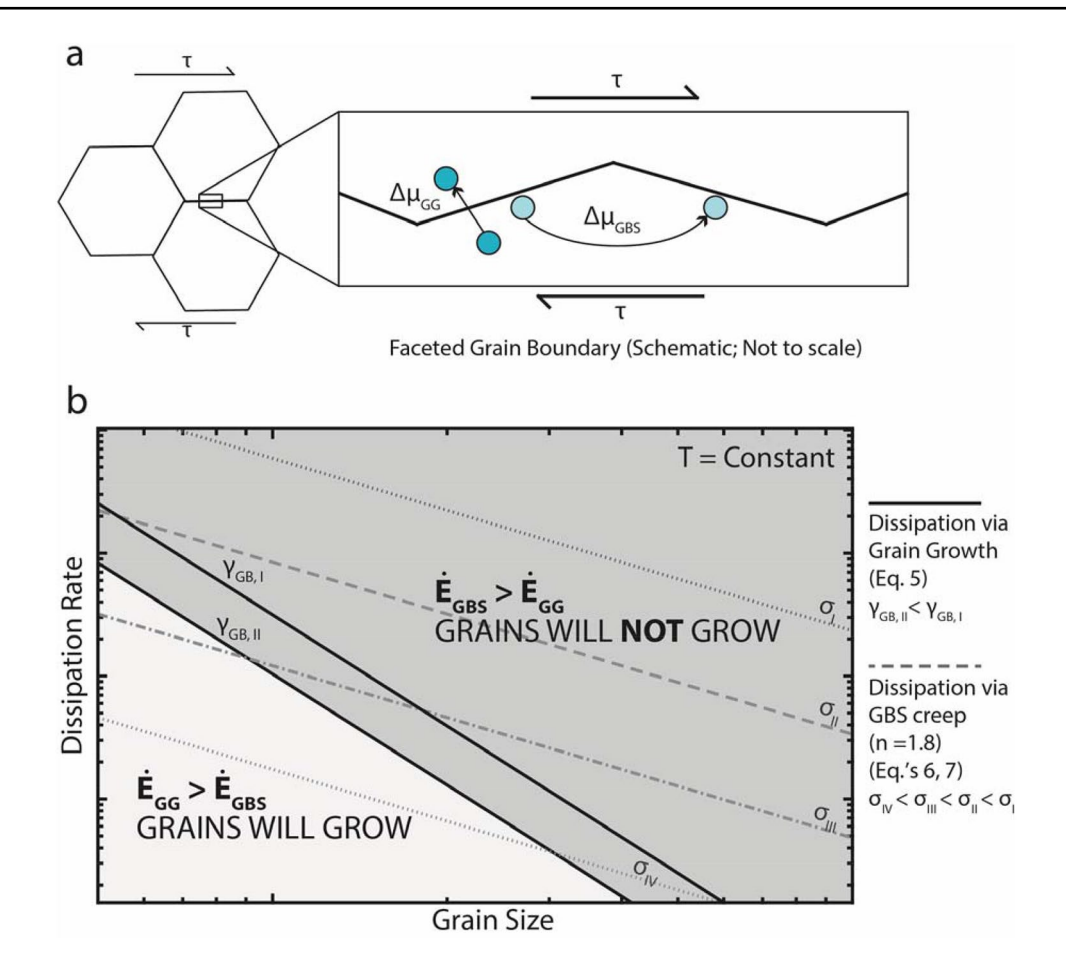


Fig. 1 a Combined driving potentials for grain growth ($\Delta \mu_{GG}$) and boundary-sliding rheology that is rate-limited by chemical diffusion $(\Delta \mu_{GBS} \equiv \Delta \mu_{Tr})$ for a single-phase, polycrystalline material having faceted grain boundaries and subjected to a persistent shear stress, τ . **b** Schematic log-log plot (isothermal, isobaric) comparing the energy-dissipation rates of grain growth (\dot{E}_{GG} ; Eq. (5)) and of grain-size-sensitive plastic deformation, specifically GBS that is rate-limited by boundary-sliding kinetics, incorporating the stress

and grain-size sensitivity parameters (exponents) of Goldsby and Kohlstedt (2001) ($\dot{E}_{Pl} \equiv \dot{E}_{GBS}$; Eqs. (6) and (7)). Following Onsager's (1931) model of maximum-power dynamics, this space is divided between conditions where the rate of energy dissipation by grain growth exceeds that of GSS creep (fine grain size and low stress) and where that of creep exceeds that of grain growth (larger grain size and higher stress). The dividing boundary (heavy solid line) is affected by the grain-boundary energy, γ_{GB}

sense). Diffusion creep (i) and GBS that is rate-limited by the boundary-sliding kinetics (ii(a)) are the mechanisms whose rates are sensitive to the grain size.

Rate-sensitive, thermally activated plastic flow at a steady state is described by the semi-empirical Mukherjee-Bird-Dorn equation (Mukherjee et al. 1969):

$$\dot{\varepsilon}_{Pl,i} = \frac{A_i \sigma^{n_i}}{d^{p_i}} \exp\left(\frac{-Q_{Pl,i}}{RT}\right),\tag{7}$$

where A_i is a constant that incorporates aspects of microstructure other than grain size (including, in this formulation, any effects of chemical potentials), n_i is the stress exponent, p_i is the grain-size sensitivity, and $Q_{Pl,i}$ is the activation enthalpy for the flow mechanism. The subscript i in Eq. 7 refers to the dominant kinetic mechanism (i.e., mechanisms (i) through (iii) articulated above, with mechanism (iv) being neither rate-sensitive nor thermally activated). Values of n and p are used to identify the active—that is, kinetically dominant—deformation process, and the value of Q_{nl} characterizes the rate-limiting kinetic step of that dominant process. For GBS that is rate-limited by the boundary-sliding kinetics, which is our interest here, n = 1.8 and p = 1.4(Goldsby and Kohlstedt 2001). The energy dissipation rate associated with thermally activated plasticity is calculated by substituting Eq. (7) into Eq. (6).

We present in Fig. 1b a schematic log-log graph where the grain size is plotted versus energy dissipation rate for an isothermal condition. This variable space is divided into two regions, one where the energy dissipation rate of grain growth (Eq. (5)) exceeds that of steady-state plastic flow by boundary-sliding-limited GBS (mechanism ii(a)) and one



where the opposite occurs. The rates are equal at the boundary between regions. The postulate of this work is that, for a given set of (σ, d, T) potentials (d representing the volume potential associated with grain boundary energy, cf. Equation (1)), specimens deforming in GSS creep will experience grain growth—and consequent increase in effective viscosity with time (strain)—only for initial conditions where the grain size is sufficiently small that $\dot{E}_{GG} > \dot{E}_{Pl}$.

The license for preparing Fig. 1b, and for arguing its significance, is the postulate of maximum power dissipation in non-equilibrium thermodynamics. Onsager (1931), in his Nobel-Prize work on transport coefficients, as well as others (e.g., Odum and Pinkerton 1955; Ziegler 1958; Ziegler and Wehrli 1987; Hillert and Agren 2006) have argued that systems pushed (and sustained) from equilibrium will evolve so as to maximize the rate of energy dissipation (or entropy production). There are caveats. First, the perturbed system must remain in the "linear" dynamic regime, i.e., that referred to by Prigogine (1997, p. 66) as the "thermodynamic branch" of disequilibrium. Second, the evolving system must be characterized by "local equilibrium," that is, the change (lowering) in Gibbs free energy of the system with each atomic/molecular "step" in the dynamic response be significantly less than the product k_BT , where k_B is Boltzmann's constant (e.g., Kingery et al. 1976, p. 230; Schmalzried 1995, Ch.5). Both these caveats are met for the arguably "gentle" processes of grain growth and rate-dependent plasticity. An additional constraint must be considered, however: in competing kinetic (dissipative) processes, the relative activation energies of the initial kinetic steps influence the overall kinetic path (e.g., Kingery et al. 1976, p. 382). Consider, for example, the solidification of a liquid at constant temperature and pressure: to form a metastable assemblage, there must be sufficient undercooling to allow for the reaction and the system of atoms must cascade in free energy to a state that is not the lowest one available. This situation is only tenable if the first kinetic step—overcoming the activation energy barrier for nucleation—is easier for the metastable crystalline form than for the stable form (e.g., Cooper et al. 1991): the relative values of $\Delta_r G$ (Gibbs energy of reaction; $|\Delta_{r}G_{metastable}| < |\Delta_{r}G_{stable}|$) have little effect.

Applying this insight to the problem at hand, the first kinetic step in grain growth and in sliding-limited GBS is arguably identical: detachment of ions (or, in the case of ice, perhaps of H₂O molecules) from the boundary. This being the case, the first-kinetic-step constraint is neutralized, allowing the rest of the response kinetics for grain growth and GSS creep to "compete." The fact that the system is attempting to "discover" (by thermal sampling) a texture that facilitates the highest rate of energy dissipation, combined with the fact that the grain-size sensitivity of the dissipation rate is greater for creep, allow the direct comparison of Eqs. (5) and (6), which is represented schematically in Fig. 1b.

Experimental approach

Specimen preparation and deformation/annealing experiments

Experimental specimens were prepared specifically to explore grain size evolution and were thus fabricated with different initial grain sizes. Two distinct methods were utilized: hot-pressing and pressure-cycling (Stern et al. 1997; Goldsby and Kohlstedt 2001). Hot-pressed ice is fabricated by nebulizing deionized water in the air and directing the spray into liquid nitrogen (LN2). The resulting slurry is then sieved in LN2 to obtain the desired grain size. Sieving is performed under N₂ gas so that atmospheric CO₂ and water vapor do not deposit onto the sieved material. The resulting powder is packed into a cylindrical vacuum mold and hot-pressed in dry ice (195 K) at 100 MPa for 2 h. The resulting sample is fully dense and possesses a grain size approximately equal to the particle size of the initial sieved powder (Goldsby and Kohlstedt 1997; Caswell et al. 2015; Prior et al. 2015). By this method, we produced 1-cm diameter, 2-cm length cylindrical specimens of grain sizes in the range 25–70 µm.

Pressure-cycled ice is prepared in an identical manner to hot-pressing except for a sequence of high-pressure/lowpressure cycles prior to the final hot-pressing (Stern et al. 1997). Each pressure cycle begins by increasing the (nominally hydrostatic) stress on the sample to 250–300 MPa, which initiates a phase transformation from ice Ih to the high-density polymorph, ice II. The sample is held at 250–300 MPa for 5 min to allow the phase transformation to complete before the pressure is rapidly released. During the phase transformation back to ice I, the kinetics of nucleation dominate relative to those of grain growth and a high density of ice I nuclei is produced. These nuclei then grow to produce specimens of extremely fine grain size (5–10 μm). The pressure-cycling process is repeated three to six times, with greater numbers of cycles producing finer grain sizes. In this manner, we produced 1-cm diameter, 2-cm length cylindrical specimens with mean grain sizes $\sim 9-30 \mu m$. All specimens were stored in dry ice (195 K) between fabrication and use in experiments, generally for less than 48 h.

The experiments involved characterizing and comparing three types of specimens: (i) starting material (undeformed/unannealed), (ii) the deformed material, and (iii) material that was annealed under identical (and simultaneous) time-temperature (thermal) conditions as the deformed material without being subjected to deviatoric stress. In what follows, the first type of material is described as "Starting," the second as "Deformed" and the third as "Thermal." Prior to each experiment, a section of



the starting material was cut from the cylindrical sample and placed directly into a liquid nitrogen storage dewar (77 K) for later microstructural comparison; these specimens are the "Starting" material. A second section of the sample was placed inside the apparatus, adjacent to the deformation specimen but not subject to load; these specimens are the "Thermal" specimens.

The deformation experiments reported here arise from two different apparatus. The first utilized a dead-weight creep device described elsewhere (Goldsby and Kohlstedt 1997). The second utilized a computer-controlled, servo-mechanical apparatus (Instron Model 1361) modified by the addition of an ethanol-bath cryostat that maintains sample temperature to a precision of ± 0.5 K (Fig. 2). Strain and strain rate in the specimen were determined by measuring displacement between ceramic plates abutting the specimen using a displacement-voltage transducer (direct current differential transformer—DCDT). Specimen temperature was measured by a Type-T (copper–constantan)

thermocouple embedded in the uppermost of these plates. The data acquisition system employed averaging to mitigate electronic noise: though data were recorded at 5 Hz, each recorded data point was an average of 1000 samples collected at 5 kHz. Including this averaging and analog-to-digital conversion, strain resolution was 1×10^{-7} . Load was measured by a 2.2 kN-capacity load cell with a resolution of 0.035 N. The computer-controlled load setpoint was adjusted every ~24 h to maintain constant stress on the sample, assuming constant-volume deformation of a cylindrical sample.

The experiments were designed to fall into two groups according to the theory presented in Sect. Theoretical considerations: one in which the Starting grain size and initial differential stress $(\sigma_1 - \sigma_3 \equiv \sigma_1)$ condition favored grain growth in the deforming specimen and the other in which, again because of the selection of initial d and σ_1 , grain growth is anticipated to be inhibited. Dissipation rates by grain growth were calculated using Eq. (5). Deviatoric

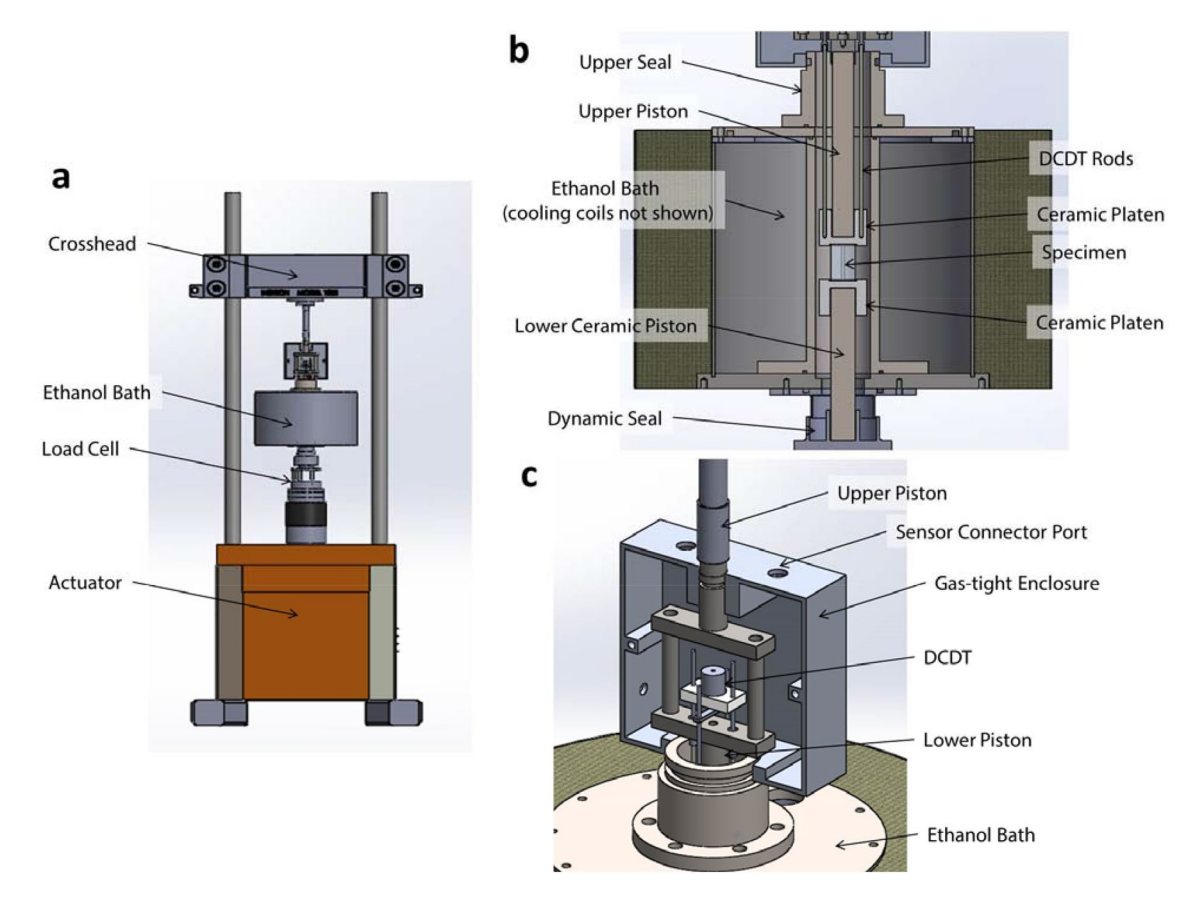


Fig. 2 The servomechanical apparatus employed in the majority of experiments (schematic). **a** Full assembly, including Instron 1361 load frame and actuator, ethanol bath cryostat, and extensometer. **b** The sample assembly within the cryostat. The distance between two ceramic (MacorTM) platens abutting the ends of the specimen is measured/monitored by a direct-current differential transformer (DCDT), which is located outside the cryostat; the DCDT is connected to

the platens via long ceramic rods, "floating" so as to provide temperature-fluctuation and -gradient compensation. Small "thermal" specimens (not to experience deformation) rest on the bottom platen beside the deformation specimen. ${\bf c}$ Extensometer electronics housing. The housing is sealed; N_2 gas is passed through the housing to prevent frosting of the electronics



stress was adjusted to control the dissipation rate by creep (Eq. (6)).

Deformed specimens were subjected to deviatoric stresses of $\sigma_1 = 0.25-1.65$ MPa at temperatures of 240 K for 4–12 days, the initial stress conditions selected to place a specimen in either the growth or no-growth regime as described above. Specimens utilized to explore the question of grain growth were additionally interrogated for steadystate and transient creep responses as well as low-frequency attenuation behavior (the latter presented elsewhere). As a result, many Deformed specimens experienced multiple, contiguous segments of deformation (i.e., stress steps), each of which accumulated sufficient strain to achieve steady-state flow behavior ($\varepsilon \ge 0.02$). Thus, in the interest of addressing the grain-growth/GSS-deformation question at hand, deformation segments beyond the initial one were designed to be in the "no-growth" regime, based on the starting grain size. A consequence is that the microstructures of Thermal specimens are being compared with Deformed specimens having a somewhat more complex history.

At the start of each experiment, the deformation and Thermal specimens were transferred from dry ice to the apparatus, which was initially equilibrated at 195 K. The apparatus then passively warmed to the experiment temperature (240 K), allowing the specimens to equilibrate thermally over the course of 24 h. A low, controlled deviatoric stress (250–400 kPa, depending on estimated initial grain size) was applied to the to-be-deformed specimen during equilibration to facilitate "bump-free" initiation of deformation experiments and, again based on our theoretical assumptions (Sect. Theoretical considerations), suppress grain growth in appropriate specimens during the thermal equilibration timeframe.

Deformed and thermal specimens were quenched simultaneously in LN2 immediately following each experiment.

In one experiment a "Grow" specimen was also studied. This specimen was sectioned from a Deformed specimen after deformation and reinserted into the cryostat for additional, stress-free annealing at 240 K for 48 h. This specific experiment allowed us to evaluate whether cavitation, potentially induced by GBS, influenced grain size evolution in deformed samples.

Microstructure analysis

Microstructural analyses were performed via reflected-light optical microscopy and cryogenic electron backscatter diffraction (EBSD) in scanning electron microscopy. Because microstructural analyses were conducted several weeks after the completion of mechanical experiments, specimens were stored in an LN2 dewar (77 K; – 196 °C) between experiments and microscopy.

EBSD was performed on a Zeiss Sigma field-emission scanning electron microscope at the Otago Center for Electron Microscopy (University of Otago, Dunedin, New Zealand) (Prior et al. 2015). Sections for analysis were cut from experimental specimens using a band saw and bonded to copper SEM adapters by a very thin (~100 μm) melt layer, which forms a strong bond while maintaining sample temperature below 223 K (- 50 °C). The sample surface was shaved flat in a cryogenic microtome at 243 K (- 30 °C) before insertion into the SEM via a nitrogen-filled airlock that prevented frost accumulation on the samples.

Optical microscopy was conducted in a cold room at Lamont-Doherty Earth Observatory (Palisades, New York, USA). Sections for analysis were cut from each specimen using a razor blade in a cooler over LN2. Sections were then transferred to the cold room (256 K; – 17 °C) where they were bonded to a glass slide with drops of water. Specimens were prepared for microscopy by shaving a flat surface with a microtome, then allowing the shaved surface to etch via sublimation in the cold room for 1–2 min to produce etched grain boundaries (Caswell et al. 2015). Images were collected with a Leica DM2700 reflected-light microscope in the cold room.

Image analysis was conducted using the NIH software ImageJ. Grain size was measured by the line-intercept method, applying a multiplicative factor 1.5 to account for geometric effects (Exner 1972). Grain sizes reported are averages taken from multiple images of each sample. EBSD data were analyzed using the Channel 5 HKL software package.

Results

Table 1 presents a synopsis of the experiments and results. To facilitate presenting experimental results graphically, we have binned the data based on the initial (Starting) grain size of a specimen; the bins are "Fine" ($d \le 10 \mu m$; represented in graphs as open and filled circles) and "Coarse" ($d \ge 20 \mu m$; squares). In the table, grain sizes are presented as the mean \pm one standard deviation.

Mechanical data

The steady-state stress and strain rate pairs from our mechanical tests are presented in Fig. 3, with material identified by its starting (i.e., as fabricated) average grain size, binned as indicated above. All measured steady-state strain rates are consistent (within a factor of three) with those predicted by the composite rheology of Goldsby and Kohlstedt (2001), which is indicated by gray lines for comparison to the data in Fig. 3. The composite rheology curves indicate the transition in ice creep from sliding-limited GBS at low stress (slope on



Table 1 Grain sizes for starting, deformed and thermal specimens; differential stress (σ_1) ; maximum energy dissipation rates by grain growth $(\dot{E}_{GG};$ predicted via Eq. (5)) and by plastic deformation via

sliding-limited GBS (\dot{E}_{Pl} ; measured via Eq. (6)); and prediction for grain growth during deformation

| Experiment code | Grain size Starting (μm) | Grain size range sym- bol* | Grain size Deformed (µm) | Grain size Thermal (µm) | Dur. [†] (days) | σ_1^{\ddagger} (MPa) | \dot{E}_{GG}^{\S} (J m ⁻³) | \dot{E}_{Pl}^{\ddagger} (J m ⁻³) | Growth expected? |
|-----------------|-----------------------------|----------------------------------|--------------------------------|----------------------------|-----------------------------|-----------------------------|--|--|------------------|
| GVF1 | 29.9 ± 5.4 | | 24.5 ± 5.4 | 66.8 ± 21.5 | 4 | 1.0 | 0.0292 | 0.2600 | N |
| AM2 | 63.0 ± 9.0 | | 82.9 ± 13.9 | 102.5 ± 22.7 | 12 | 0.4 | 0.0031 | 0.0108 | N |
| AM7 | 41.0 ± 4.4 | | 41.4 ± 6.5 | 70.8 ± 8.1 | 12 | 0.4 | 0.0113 | 0.0300 | N |
| SD4 | 33 ± 3.2 | | 34 ± 7.3 | N/A | 11 | 0.93 | 0.0217 | 0.1434 | N |
| SD8 | 33 ± 3.2 | | 41 ± 6.4 | N/A | 4 | 1.6 | 0.0217 | 0.3240 | N |
| AVF2 | 6.4 ± 1.6 | 0 | 7.8 ± 1.6 | 12.4 ± 4.2 | 5 | 0.25 | 2.9750 | 0.0210 | Y |
| AVF1 | 8.7 ± 2.8 | 0 | 18.9 ± 4.4 | 20.8 ± 4.7 | 7 | 0.5 | 0.1155 | 0.0440 | Y |
| GVF5 | 9.7 ± 5.2 | 0 | 11.5 ± 2.0 | 26.2 ± 3.4 | 11 | 0.25 | 0.8546 | 0.0015 | Y |
| AVF3 | 8.2 ± 0.5 | 0 | 16.9 ± 3.4 | 20.1 ± 3.3 | 9 | 1.0 | 1.4145 | 0.0520 | Y |

All experiments at T = 240 K

[§]Calculated (Eq. (5)) with $K = 1 \times 10^{-15} \text{ m}^2 \text{ s}^{-1}$, $\gamma_{GB}^{ice-l} = 0.065 \text{ J m}^{-2}$ and t = 1 s

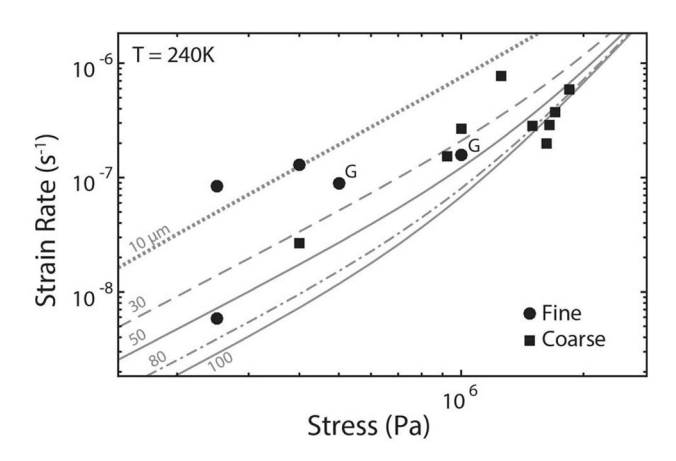


Fig. 3 Steady-state strain rate vs. differential stress for our experimental specimens deformed in uniaxial compression at 240 K. For reference, the composite flow law of Goldsby and Kohlstedt (2001) is plotted as gray lines for grain sizes comparable to our Deformed specimens. The symbol sizes are defined based on the Starting—not final—grain size in the specimen; thus, fine-grained specimens that experienced grain growth are still labeled as "Fine" despite reduced strain rates indicative of grain growth during some experiments. Stress segments during which statistically-significant growth occurred are indicated by the letter "G" to the upper right of the corresponding symbol

the log-log plot of n=1.8; cf. Equation (7)) to dislocation creep at higher stress (n=4); the transition is most easily perceived in the concave-up topology of the curves representing the flow of specimens of grain size exceeding 50 μ m. As noted in Specimen Preparation and Deformation/Annealing Experiments, multiple stress segments were conducted in some experiments, which accounts for the number of data

points exceeding the number of specimens. The stress- and grain size-sensitivities of steady-state strain rate perceived from this graph should be approached with caution, however, because several experiments were conducted under conditions anticipated (by the postulate articulated in Sect. Theoretical considerations) to favor grain growth. The resulting stress exponent is therefore a convolution of stress and grain size variations. For the experiment with most stress segments and the least measured change in grain size (SD4; Table 1), the observed stress exponent is n = 1.6.

The rheology is distinctly sensitive to grain size, though the number of data points is small: the average value of the grain size exponent (Eq. (7)) in the subset of experiments crept at the same stress is p = 2.1.

Microstructures

Optical micrographs of representative samples are shown in Fig. 4. Two-grain boundary morphologies are seen in the deformed specimens depending upon whether grain growth occurred during the experiment. This variation is exhibited in the figure, in which the left-hand column (a-c) illustrates a specimen (GVF1; cf. Table 1) deformed under conditions expected to inhibit grain growth, while the right-hand column (d-f) illustrates a specimen (AVF3) deformed under conditions favoring simultaneous grain growth.

It is apparent from visual inspection of Fig. 4a and b that grain size remains similar between the Deformed specimen and the Starting material in Specimen GVF1. In this and similar experiments, the Deformed specimen exhibits numerous four-grain junctions (black arrows,



 $^{^*\}Box \equiv \text{Coarse}; \bigcirc \equiv \text{Fine}$

[†]Total time duration of deformation/thermal experiment

[‡]First-segment, lowest-stress and corresponding, minimum plastic-deformation energy dissipation rate

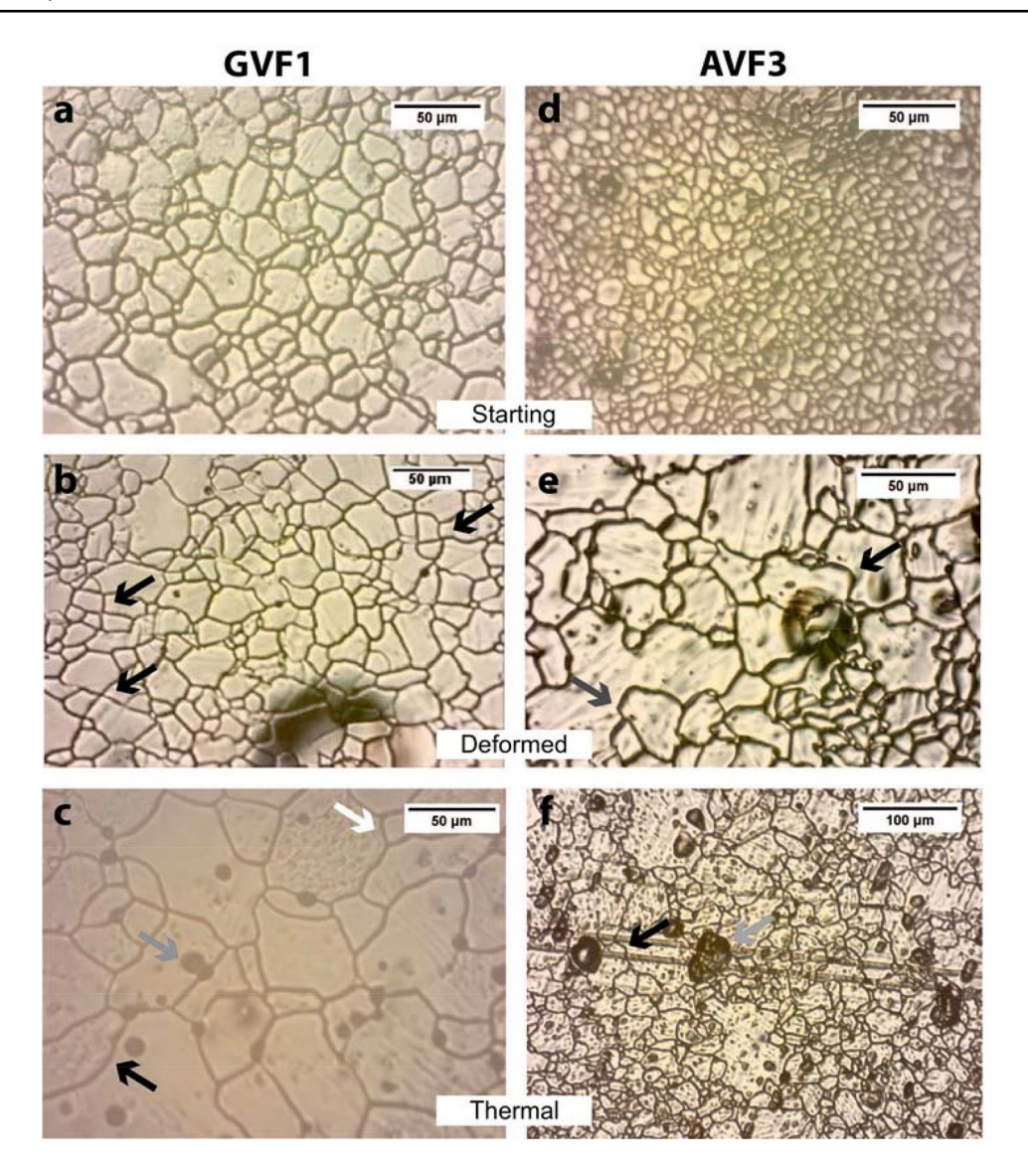


Fig. 4 Reflected light micrographs of experimental specimens. The column on the left represents an experiment (code GVF1; see Table 1), conducted under conditions in which grain growth is inhibited in the deforming specimen. The column on the right represents an experiment (code AVF3), conducted under conditions expected to allow grain growth. **a** GVF1 Starting material: $d=29.9\pm5.4$ µm. **b** GVF1 Deformed specimen ($\sigma_I = 1$ MPa, $\varepsilon = 0.101$, 240 K, duration 3.7 d; compression axis perpendicular to image): $d=24.5\pm5.4$ µm. Grain boundaries are generally straight, and numerous four-grain junctions are visible (black arrows), consistent with a GBS texture. The grain size is unchanged from the starting material. c GVF1 Thermal specimen: $d=66.8\pm21.5$ µm. Boundaries are concave-in on large grains (black arrow) and concave-out on small grains (white

arrow), a texture associated with normal grain growth. Dark spots are frost accumulated on this specimen during microscopy (gray arrow). **d** AVF3 Starting material: $d = 8.2 \pm 0.5 \mu m$. **e** AVF3 Deformed specimen (σ_1 =0.4 MPa, ε =0.121, 240 K, duration 9.4d; compression axis perpendicular to image): $d=16.9\pm3.4$ µm. Numerous curved boundaries (e.g., black arrow) indicate a growth texture. Several cuspate boundaries are evident (gray arrow). f AVF3 Thermal specimen: $d=20.1\pm3.2$ µm. (Note that the magnification in this image is half that in (e)). Numerous, highly curved grain boundaries are visible. Some boundaries exhibit cusps (black arrow). Frost, accumulated during microscopy, forms dark blots on the surface (gray arrow). Scratches from the microtome blade cross the image from left to right

Fig. 4b). Many grain boundaries are linear, showing very little evidence for migration. Thermal specimens (e.g., Fig. 4c) exhibit highly curved grain boundaries. Small grains generally possess convex-outward grain boundaries (white arrow), while large grains have concave-inward boundaries (black arrow). Comparison of Fig. 4a and c clearly illustrates a marked increase in grain size in the Thermal specimen.

Figure 4d and e show the starting material and deformed specimen for a single experiment conducted under conditions in which grain growth is expected. It is clear from visual inspection that the grain size in the deformed specimen



is much larger than that in the starting material. In contrast to the deformed specimen shown in Fig. 4b, grain boundaries are generally curved (e.g., black arrow, Fig. 4e). A few cuspate boundaries are observed, suggesting pinning of the boundaries in some locations (gray arrows, Fig. 4e). The Thermal specimen for the same experiment also shows highly curved boundaries (e.g., black arrows, Fig. 4f), convex-out small grains, concave-in large grains, and slight cusps on some grain boundaries (gray arrow, Fig. 4f).

Though sliding-limited GBS in ice is geometrically accommodated by the glide of basal dislocations, the microstructures of our deformed samples show very little—to first order, none—formation of low-angle (subgrain) boundaries. In addition to the dearth of shallow sublimation features seen in reflected light images (Fig. 4), EBSD data from deformed specimens reveal few low-angle boundaries (cf. Caswell et al. (2015)).

Grain sizes in all samples—Starting, Deformed and Thermal—are presented in Fig. 5. Error bars represent one standard deviation. We note that the broad error bars in Fig. 5 are expected for the analysis of a three-dimensional phenomenon via random, two-dimensional slices (Exner 1972). The question of grain growth, however, is a binary one and thus the means presented in Fig. 5 are significant. Thermal specimens (white symbols, Fig. 5) show continuously increasing grain size with annealing time, which is presented in Fig. 6a and b, where the values of $(d^2 - d_a^2)$ are plotted versus time. Data for the Thermal specimens are consistent with the model for normal grain growth, and can be fit via linear regression to the dynamics equation (Eq. (3)) to discern the (temperature-sensitive) kinetic growth constant K. For the condition where we (logically) force the regression through the origin, the values determined are: (a) for Fine grain-sized Thermal specimens, $K = 5(\pm 1) \times 10^{-16}$ $\rm m^2 s^{-1}$ (correlation coefficient r = 0.931; this K is represented as the slope of the dotted line in Fig. 6a and b); (b) for the Coarse grain-sized Thermal specimens, $K = 6(\pm 1) \times 10^{-15}$ $\rm m^2 s^{-1}$ (r=0.802), and (c) for Fine grain-sized Deformed specimens, $K = 4(\pm 1) \times 10^{-16} \text{ m}^2\text{s}^{-1}$ (r = 0.798). (The precision indicated for the values of K are the standard error for the respective linear regressions based on the measured average values of grain size (Walpole and Myers 1972, p. 286)). The "Grow" specimen (a piece of Deformed specimen GVF5, which was annealed following deformation as described in Sect. Theoretical considerations), is shown as a diamond in Fig. 6a and b. This specimen shows an increase

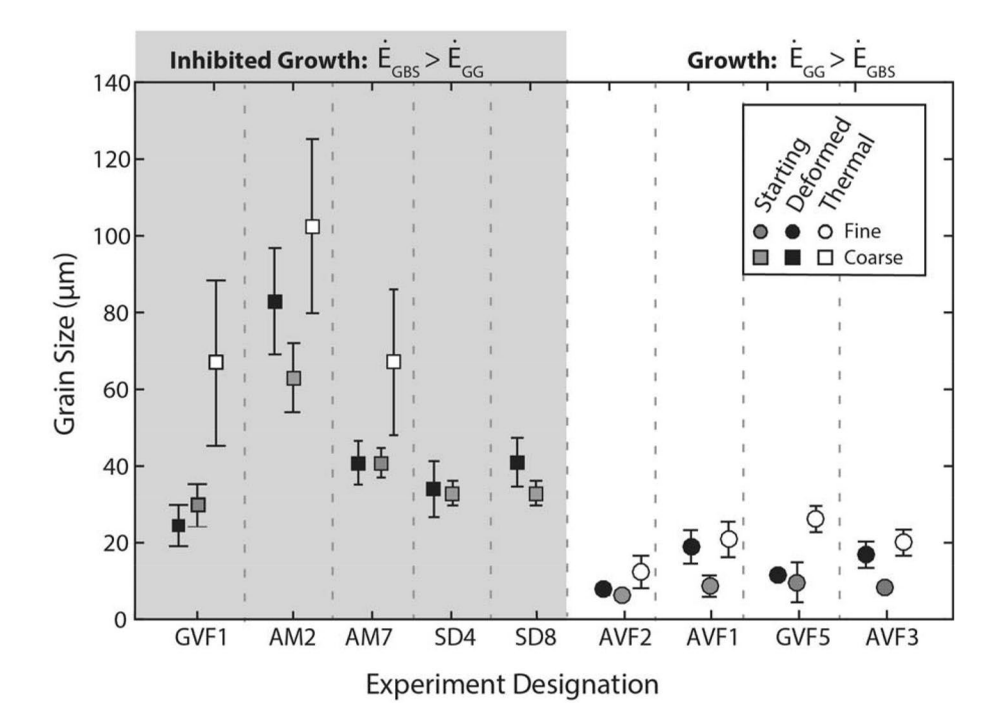


Fig. 5 Grain sizes of all specimens. The experiments are divided into two groups: the five experiments on the left are those in which the Deformed specimen was subjected to a stress (σ_1) sufficiently large such that-given the Starting grain size-the energy dissipation rate due to plasticity exceeded that due to grain growth $(\dot{E}_{GBS} \equiv \dot{E}_{Pl} > \dot{E}_{GG})$; as such, no grain growth during deformation was anticipated. The experiments on the right were conducted under conditions favoring grain growth during deformation

 $(E_{GG}>\dot{E}_{GBS}\equiv\dot{E}_{Pl}).$ As indicated in the key, symbol shape represents the Starting grain size bin; symbol shading identifies Starting from Deformed from Thermal specimens. Specimen symbols for each experiment are offset for clarity. Error bars represent one standard deviation around the mean grain size; if error bars are not present, the error is smaller than the symbol size. (Thermal specimens were not included in experiments SD4 and SD8.)



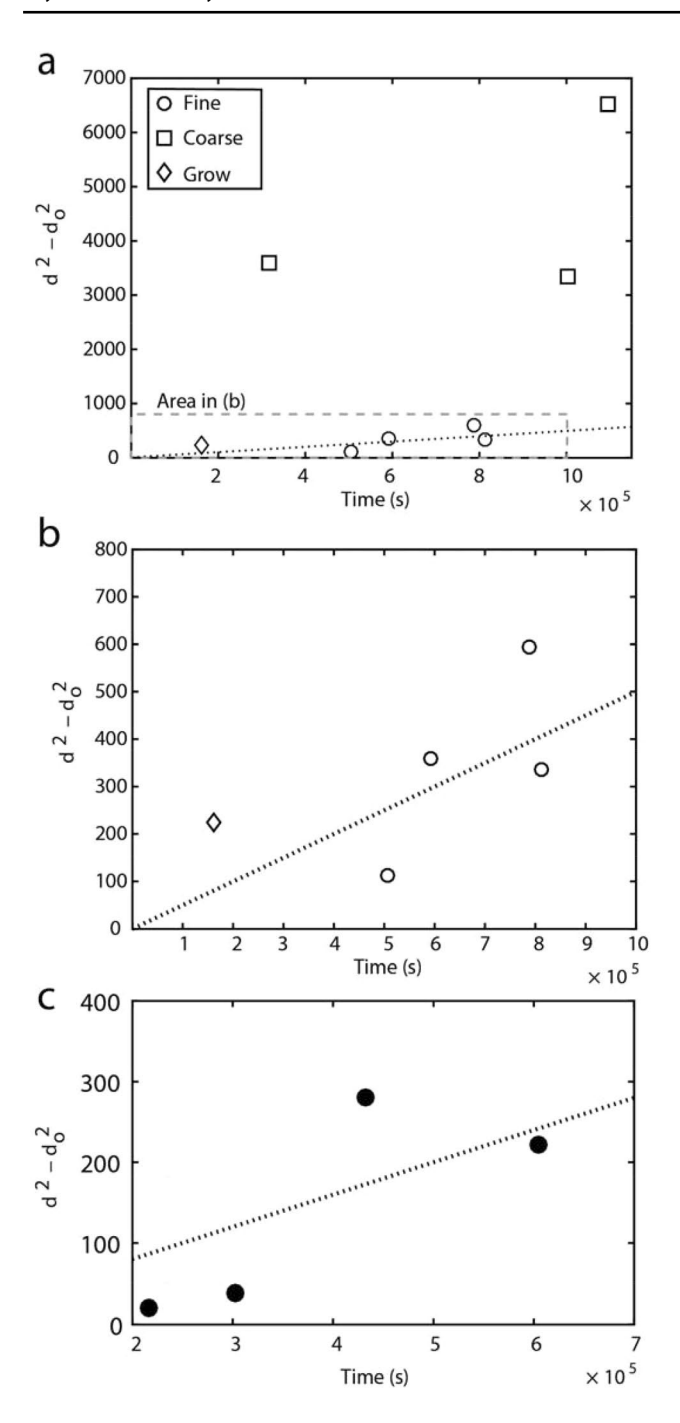


Fig. 6 Grain growth kinetics: the quantity $(d^2 - d_o^2)$, in units μm^2 , is plotted against time (cf. Equation (3)). **a** and **b** Grain growth in Thermal specimens. Two trends are observed, indicating different grain growth kinetics for our Fine grain-size specimens relative to our Coarse grain-size specimens. The Fine grain-size specimens, shown in (b), produce a growth-rate constant $K=5\times10^{-16}$ m²s⁻¹, which plots as the dotted line. **c** Grain growth in those Deformed specimens—all in the Fine grain-size category—for which $\dot{E}_{GG} > \dot{E}_{GBS} \equiv \dot{E}_{Pl}$. Growth of these specimens produces a grain growth constant $K=4\times10^{-16}$ m²s⁻¹ (dotted line), which, given the experimental scatter, is nominally the same as that for Thermal specimens

in grain size consistent with the trend observed for the Fine grain-size Thermal specimens.

In contrast to the Thermal specimens, the critical result presented in Fig. 5 is that the grain size in the Deformed specimens fall clearly into two groups depending on whether the deformation conditions were expected to inhibit grain growth according to the theoretical considerations presented in Sect. Theoretical considerations; this result will be explored in depth in the Discussion.

Discussion

Comparison of deformation and grain growth results to similar studies on ice

The deformed specimens exhibit both microstructures and effective viscosity consistent with the dominant deformation mechanism being grain boundary sliding that is rate-limited by the sliding along the grain boundary (mechanism (ii)(a) in Sect. Theoretical considerations). Evidence for slidinglimited GBS includes the low, but non-Newtonian stress exponent (n = 1.6; cf. Goldsby and Kohlstedt (2001) andFig. 3), and deformation microstructures evincing straight grain boundaries and numerous four-grain junctions, which are considered diagnostic of grain switching events during GBS (Ashby and Verrall 1973; Langdon 1991; Goldsby and Kohlstedt 1997). Thus, the rheological response of polycrystalline ice in our experiments is consistent with the chemical potential difference (and potential gradient with characteristic distance being the grain size) as presented schematically in Fig. 1a.

Comparing the kinetic grain-growth constants K (Fig. 6) experimentally determined here to values reported elsewhere demonstrates the challenge—widely experienced—of measuring the kinetics of grain growth and grain boundary mobility (e.g., Evans et al. 2001; for ice, cf. Fan et al. 2021). The value that we measured for the growth constant in the Fine grain-sized Thermal specimens— $K = 5 \times 10^{-16} \text{ m}^2\text{s}^{-1}$ —is a factor of ten to a factor of thirty slower than those reported by Arena et al. (1997) and Azuma et al. (2012), respectively, for "bubble-free" ice. Nevertheless, our value matches well with those measured by both these studies for polycrystalline ice containing a small concentration of broadly dispersed fine bubbles (which serve to pin grain boundaries and so slow the kinetics of grain growth). While no bubbles are readily apparent in the microstructural study of our specimens (to a resolution of $\sim 1 \mu m$), we do note that some grain boundaries in the initially Fine grain-sized Thermal specimens exhibit evidence of pinning (e.g., grain boundary cusps in Fig. 4f). A small concentration of extremely small bubbles along grain boundaries, perhaps remnant from the sample fabrication process, may therefore be the source of



the sluggish grain growth observed in the Fine grain-sized Thermal specimens. And while it borders on speculation, ice II, the cycling from which the Fine grain-sized specimens were prepared, has been demonstrated to persist as a metastable phase (e.g., Bauer et al. 2008; Nakamura et al. 2016): in the context of the strain-energy state of grain boundaries, durable, sub-micrometer particles of ice II may well characterize the texture of grain boundaries (cf. Raj 1981, for the case of glass–ceramics). Such particles would fill the same boundary-pinning role as fine bubbles.

Deformed Fine grained-sized specimens, anticipated to grow during deformation (see Sect. Theoretical considerations and below), as well as the singular, Fine grainsized (post-deformation) Grow specimen demonstrated the same growth constant—K=4 to 5×10^{-16} m²s⁻¹—as did the Fine Thermal specimens: the results are self-consistent. Significantly, the growth rate of the Grow specimen, being unchanged, indicates that no additional boundary-pinning textural differences occur because of the accumulation of strain via boundary-sliding dominant deformation.

The Coarse grain-sized specimens, manufactured without the solid-state ice I-ice II phase transformation, demonstrated a growth constant— $K = 6 \times 10^{-15}$ m²s⁻¹—that is consistent with the "bubble-free" ice I of other investigators.

Grain growth during grain size-sensitive deformation?

Evaluation of the data for both deformation and grain growth (Figs. 3, 4, 5, and 6 and discussed above) allows the evolution of the schematic presented as Fig. 1b into a quantitative dissipation-rate v. grain size dynamics "map," which we present as Fig. 7. Two boundaries are presented for energy dissipation by normal grain growth: black and black-dotted lines representing K (m²s⁻¹) = 1×10^{-16} and 1×10^{-15} , respectively, which bracket our measurements. These divide space between regions where the dissipation rate by grain growth exceeds that for GSS plastic deformation and vice versa. The map presents gray contours corresponding to the differential stress that drive deformation, using the parameterization by Goldsby and Kohlstedt (2001) (with which our data correlate). Dissipation-rate data from our experiments are arrayed on the map (cf. Fig. 3 and Table 1): for Coarse specimens, the dissipation is from flow, while for Fine specimens the dissipation is from grain growth. In that Eq. (5) reveals that dissipation by grain growth is a function of a negative power of time, we have chosen to use for Table 1 and Fig. 7 a nominally maximum value for \dot{E}_{GG} based on t=1 s.

Inspection of Fig. 7 reveals that our experimental data fall into two groups: one in which the rate of energy dissipation by grain growth exceeds that for creep, and the other in which the opposite hierarchy exists. This is by design,

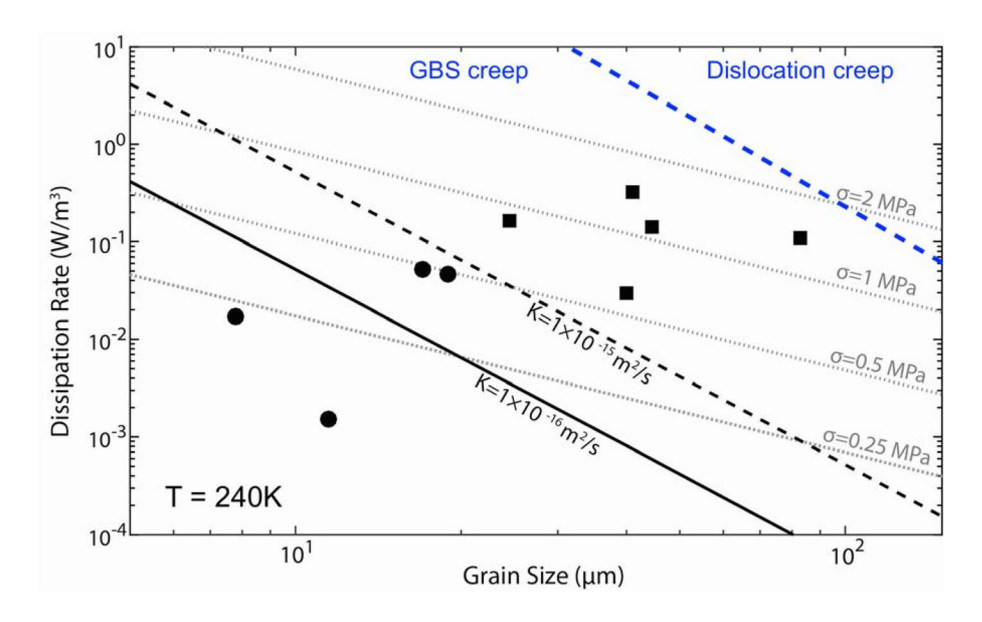


Fig. 7 Comparison of energy dissipation rates by boundary-sliding-limited GBS (gray dotted lines, Eqs. (6) and (7)) and normal grain growth (heavy black lines, Eq. (5)) as a function of grain size; T=240 K. Creep dissipation curves are based on the flow-law parameters of Goldsby and Kohlstedt (2001), as is the noted transition from GBS to dislocation creep. The magnitude of differential stress for each plasticity dissipation line is given at right. Grain growth dissipation employs γ_{GB}^{ice-l} =0.065 J m⁻². Grain growth dynamics for

two values of the rate constant K (Eq. (3)) that bracket our experimental findings are shown. The data symbols follow the usage of earlier figures. In our experiments, the specimens noted with black circles experienced grain growth during GBS creep while those noted with black squares did not (cf. Fig. 5). (One would anticipate grain growth occurring in specimens deformed within the dislocation creep regime.)



of course, to evaluate the model we have articulated: grain growth is expected to occur in one group but not the other.

The first group includes Coarse grain-sized specimens subjected to loading conditions under which the energy dissipation rate via GSS creep is greater than that by grain growth. Grain growth is expected to be suppressed in these deforming specimen and, returning to Fig. 5, we see that this group (which includes experiments GVF1, AM2, SD4 and SD8—Table 1) corresponds exactly to those observed to have suppressed grain growth. The best example of this behavior is experiment GVF1, for which the Deformed specimen and Starting material have nearly identical grain size while the Thermal specimen, which was subjected to identical time—temperature conditions as the deformed specimen, has a final grain size consistent with normal grain growth (cf. Arena et al. 1997; Azuma et al. 2012).

In the experiments with Coarse grain-sized specimens SD4 and SD8 (Fig. 5; Table 1), fixturing was unavailable to include a Thermal specimen. Nevertheless, these data provide a compelling case for suppressed grain growth during GSS deformation. For specimen SD4, Deformed and Starting specimens have essentially identical grain sizes ($\sim 33 \mu m$) despite a 240 K deformation experiment that encompassed a total elapsed time of nearly 11 days. By comparison, applying Eq. (3) with the grain growth constant measured for Thermal specimens of Coarse grain size ($K = 6 \times 10^{-15} \text{ m}^2 \text{s}^{-1}$) yields a predicted final grain size from normal grain growth of 155 μm . Similarly, a Thermal specimen for experiment SD8—a 240 K deformation experiment of approximately four days duration—would be expected to have a normal grain growth final grain size of 95 μm .

The Deformed specimen for experiment AM2 exhibits a grain size between that of the Starting and Thermal specimens. Applying the value of K obtained for the thermal specimens in the Coarse grain-size fraction, the amount of grain growth indicated for the Deformed specimen would have occurred in ~3.2 days. This time is much shorter than the duration of the 240 K experiment, ~ 12 days, yet too long to be explained by any transient load alleviations during the experiment due to, e.g., frosting of the apparatus piston. Further, less than 1 µm of grain-diameter growth is anticipated for the ~ 10 min that the specimen was in the 256 K (-17 °C) environment of the cold room during microstructure analysis. We attribute the discrepancy in grain size between the Starting and Deformed specimens, thus, to heterogeneity in the original fabricated sample from which the Starting, Deformed and Thermal specimens were all derived: although the Deformed specimen shows increased grain size relative to the Starting material, the Thermal specimen exhibits a grain size that is significantly larger than either and consistent with the rate of static grain growth.

Clearly, in the dynamics regime where the dissipation rate by GSS creep exceeds that by grain growth (associated

here primarily with the Coarse grain-size specimens), grain growth is arrested or, at least, inhibited.

The second group consists of those Fine grain-sized specimens deformed at low differential stress—conditions designed to promote grain growth accompanying deformation. In these experiments, the predicted dissipation rate due to grain growth exceeds that by GSS creep. This group is indicated by Fig. 5, which demonstrates that growth occurred in each of the deformed specimens within this group. Notably, the Deformed specimens in experiments AVF1 and AVF3 possess grain sizes only slightly smaller than that in the corresponding thermal history specimens, indicating that grain growth was uninhibited as these specimens deformed.

That grain growth occurs independently of the dynamics of creep essentially has dogma status in materials science and experimental geophysics (e.g., Courtney 1990, p. 293; Karato 2008, p. 253). This is not a surprise: many investigators studying grain-size-sensitive creep (and particularly diffusion creep) in metals and ceramics (including synthesized "rock") have recorded the diminishment of (nominally) steady-state strain rate as a function of strain (i.e., time) and correlated this behavior with simultaneous grain growth. While a number of studies could be quoted, the comprehensive work of Karato (Karato et al. 1986; Karato 1989) on GSS creep and grain growth in dunite (synthetic olivine aggregates prepared from natural material) is representative. For example, in a specimen of ~10 μm initial grain size (prepared from pulverized San Carlos, AZ, peridot that was hotpressed into synthetic dunite) deformed "dry," in compression at 1300 °C and confining pressure of 300 MPa and at a nominally constant (i.e., steady-state) strain rate of 10^{-5} s⁻¹, the differential flow stress increased from approximately 4 MPa at a strain (ε) of 0.01 to approximately 20 MPa at $\varepsilon = 0.06$ (Karato et al. 1986, Experiment 4927). A conclusion of simultaneous normal grain growth accompanying diffusion creep is warranted, particularly in that the rate of grain growth matches reasonably with that for static annealing of similarly prepared aggregates (Karato 1989).

One can, however, apply the argument we have made in Sect. Theoretical considerations—and supported with our ice deformation and grain growth experiments—to contemplate these same dunite data. A 1300 °C, 300 MPa confining pressure, "dry," GSS deformation experiment (Karato et al. 1986, Experiment 4759) of many differential-stress segments in the range 45–175 MPa, with an initial grain size of 12 μ m and a total time-at-temperature exceeding seven hours, experienced but modest grain growth. Scrutinizing the lowest stress (thus lowest strain rate and corresponding energy dissipation rate by flow) with the static grain growth kinetics characterized by Karato (1989) ($K \approx 10^{-14} \, \mathrm{m}^2 \mathrm{s}^{-1}$ at 1300 °C) and employing a (high-angle) grain boundary energy of γ_{GB}^{Ol} of 0.9 J m⁻² (Cooper and



Kohlstedt 1982), the dissipation rates for both deformation and grain growth are the same at $\sim 70 \text{ J m}^{-3} \text{ s}^{-1}$. The published data suggest that higher stresses corresponded to reduced rate (or no) grain growth. Further, Karato (1989), demonstrates that those grain-growth kinetic constants measured during "dry" deformation are uniformly lower than those measured for conditions of static annealing. Consider, too, a recent experimental study, in which "wet" dunite that was partially dynamically recrystallized (i.e., large relict grains remained in the microstructure) had the growth of the recrystallized grains characterized during stress relaxation (Speciale et al. 2020): deformation in the recrystallized matter continues during relaxation and the measured kinetics of grain growth are revealed to be orders of magnitude slower than in static annealing. Taken all together, then, it is easy to imagine conditions in a geological setting where silicate rocks—even monomineralic ones—can deform by GSS creep without simultaneous grain growth.

Returning to the behavior of ice, our understanding of energy dissipation can be applied to the data of Durham et al. (2001), who studied GSS flow in ice-I at low temperatures (i.e., ~220 K) and elevated confining pressure $(P \sim 50 \text{ MPa})$. These authors observed very little grain growth in their specimens, consistent with observations made by Goldsby and Kohlstedt (1997) and with the model articulated here. Applying the analysis of Sect. Theoretical considerations, only one of their experiments—that with the finest grain size and lowest strain rate—falls near the boundary between growth- and flow-dominant dissipation rates in Fig. 7; in all others, grain growth should have been suppressed. Indeed, the authors note that the experiment whose conditions resulted in comparable dissipation rates for creep and growth (their code 420) showed a slight increase in grain size relative to the starting material, but no indication of time-dependent strengthening (i.e., consistent with grain growth) during the course of the experiment. The authors did observe strengthening in a small, additional subset of their samples, but the interpretation is nebulous. While they attributed the observed strengthening to grain growth, they were unable to derive realistic grain growth constants when fitting their data to Eqs. (3) and (7). Furthermore, the microstructures of the strengthened samples exhibited substantial irregularities, including signs of dislocation creep and grain aspect ratios of 50:1, indicative of abnormal grain growth during the ice I-II phase transition as the samples were fabricated (cf. Bennett et al. 1997; Stern et al. 1997). These microstructures indicate that rather than strengthening due to grain growth, strengthening is associated with strong fabric caused by abnormal grain growth during specimen fabrication. For samples without abnormal fabric, the Durham et al. (2001) results are fully in keeping with the model articulated here.



Geophysical implications

Because the rheology of ice is grain size-sensitive when deforming via boundary sliding-limited GBS, inhibiting grain growth restrains time (i.e., strain)-dependent strengthening. Our results suggest that when polycrystalline ice deforms via boundary sliding-limited GBS, grain size will remain constant until either (i) deviatoric stress ceases, allowing grain growth to become the sole process of free energy dissipation, or (ii) the deviatoric stress increases such that dislocation creep once again becomes the dominant mechanism, potentially leading to grain size reduction—and subsequent softening—by dynamic recrystallization.

Our results, therefore, carry implications for settings in which rheological weakening has occurred by dynamic recrystallization. Evidence from experiments and from nature indicates that shear localization and seismic slip can produce zones of dynamically recrystallized grains (i.e., mylonites) throughout the mantle and lithosphere (e.g., Karato and Wu 1993; Warren and Hirth, 2006; Kim et al. 2010; Rozel et al. 2011; Bestmann et al. 2012; Smith et al. 2013; Verberne et al. 2014). Such recrystallized zones may produce rheological weakening of the lithosphere (e.g., Rutter and Brodie, 1988), but an oft-cited criticism of models invoking this mechanism of weakening is that grain growth in the mylonitized zone limits the lifetime of weakening. Balancing growth and recrystallization then leads to the "field boundary approach" (De Bresser et al. 2001). Some authors evoke an inhibiting process to constrain grain growth; for example, both Warren and Hirth (2006) and Newman et al. (2021) (among others) suggest that permanent grain size reduction is possible due to second-phase pinning in peridotite mylonites. Our results, however, suggest that if the recrystallized grain size is sufficiently small to cause a switch to GSS rheology and the deviatoric stress is sufficient to maintain energy dissipation via GSS creep at a rate higher than that which would be produced by grain growth, the resulting zones of weakness will persist without the need for a pinning process.

The possibility of maintaining a fine grain size without second-phase pinning has profound implications for the tectonics of icy worlds and the deformation of terrestrial glaciers and ice sheets. In these settings, any stress concentration that produces a local grain size reduction sufficient to cause a switch to GSS deformation has thereby produced a zone of rheological weakness. As long as the ice continues to deform by GSS creep, this zone of weakness will persist indefinitely—a potential means of localizing strain at the margins of fast-moving ice streams or at the base of an icy satellite's lithosphere.

In particular, our results are directly applicable to the marginal zones of fast-moving Antarctic ice streams. Low basal drag due to weak basal till (e.g., Kamb 2001; Tulacyk

et al. 2001; Joughin et al. 2004) means that the margins are critical in the force balance controlling ice stream motion, and shear stresses at margins may provide as much as 93% of the force resisting downstream driving stresses (Echelmeyer et al. 1994; Whillans and van der Veen 1997). The majority of strain associated with ice stream flow is thus produced at the margins (Bindschadler and Scambos 1991; Joughin et al. 2002). Marginal ice appears to be very soft in some cases. To match a measured velocity profile across the margin of Whillans Ice Stream (Ice Stream B), Echelmeyer et al. (1994) suggested that ice within the margin is ten times weaker than that in the central part of the ice stream, though this may apply only to the region of the profile measured by the authors and may represent an extreme datum of variable ice rheology along the margins of Ice Stream B (Joughin et al. 2004). Many authors, including Echelmeyer et al. (1994), attributed such softness to shear heating and potential meltwater generation (Perol and Rice 2015; Suckale et al. 2014), though Cuffey et al. (2000) and Behn et al. (2021) point out that such enhancement is also possible by a combination of fabric development and grain size-sensitive flow. Our results suggest that it is indeed possible for grain size-sensitive flow to sustain areas of rheological weakness along ice stream margins.

The results also affect estimates of grain size in a convecting ice shell. Barr and McKinnon (2007) assumed that the dislocation component of GBS in ice was sufficient to drive dynamic recrystallization, concluding that the maximum equilibrium grain size within an ice shell is 1-10 mm. Our results here, and those of Caswell et al. (2015) indicate that the Barr and McKinnon model does not accurately capture the mechanics of grain size evolution within an ice shell. Instead, the field boundary approach may be used to estimate the initial grain size in a convecting ice shell. Such an estimate was carried out by Barr and Pappalardo (2005) who calculated, using the grain size-sensitive rheology of Goldsby and Kohlstedt (2001), that convection would not initiate within an icy Galilean satellite if initial deformation occurred by dislocation creep—i.e., for a grain size exceeding 2 cm. Using this estimate as the maximum initial grain size in a convecting ice shell at -8 °C (265 K) (Tobie et al. 2003), an initially coarse grain size $(d \sim 2 \text{ cm})$ would not experience a substantial change in grain size at a convective stress of 100 kPa. The surfaces of many icy moons are pervasively fractured, however, and the surface of Europa exhibits evidence for kilometers of displacement along strike-slip faults (e.g., Tufts et al. 1999; Hoppa et al. 2000; Nimmo and Gaidos 2002). Analogous terrestrial faults, such as the San Andreas, exhibit localized shear to the bottom of the mantle lithosphere (Ford et al. 2014), and fault slip produces recrystallization in experiments and natural settings (Bestmann et al. 2012; Smith et al. 2013). Thus, propagation of tectonic stresses to the base of an icy lithosphere may produce geologically long-lived regions of fine grain size.

Summary and conclusion

Simultaneous creep and annealing experiments have demonstrated that when polycrystalline ice deforms via grain sizesensitive (GSS) creep, grain growth is inhibited intrinsically, specifically when the free energy-dissipation rate by flow exceeds that of normal grain growth. Whether or not grain growth occurs can be predicted by calculating and comparing the dissipation rates for each mechanism following the approach presented in Sect. Theoretical considerations. For flowing, polycrystalline ice, the conditions for suppressing grain growth are met for most geologically relevant grain sizes, meaning that grain growth is expected to be suppressed in the convecting interior of an icy satellite in the outer solar system or in localized shear zones at the margins of fast-moving ice streams. It is the small driving potential for grain growth in ice, based specifically on the small value of γ_{GR}^{ice-I} (=0.065 J m⁻²)—an order of magnitude smaller than that for other (primarily ionically bonded) oxides and silicates—that allowed the separation in energy-dissipation space of grain-size-sensitive creep and grain growth to be accessed reliably in laboratory experiments. Having done so, it is straightforward to imagine the application of the discovery to other problems in crystalline rheology. Applicability of GSS creep-affected suppression of grain growth to monomineralic silicate rocks is suggested but not easily studied in laboratory settings.

Acknowledgements Greg Hirth, David Goldsby and Christine McCarthy are thanked for numerous, spirited discussions concerning many aspects of the theory explored here. The perceptive comments of Mark Behn and an anonymous reviewer improved the manuscript significantly. This research was supported financially, in part, by a grant from the Solar Systems Workings Program of the Science Mission Directorate of NASA (Grant NNX16AQ14G to R.F.C.) and by the National Science Foundation through a Graduate Research Fellowship (to T.E.C.).

References

Alley RB, Joughin I (2012) Modeling ice-sheet flow. Science 336:551–552. https://doi.org/10.1126/science.1220530

Alley RB, Gow AJ, Meese DA (1995) Mapping c-axis fabrics to study physical processes in ice. J Glaciol 41(137):197–203

Arena L, Nasello OB, Levi L (1997) Effect of bubbles on grain growth in ice. J Phys Chem B 101(32):6109–6112. https://doi.org/10.1021/jp9632394

Ashby MF, Verrall RA (1973) Diffusion-accommodated flow and superplasticity. Acta Metall 21:149–163

Austin NJ, Evans B (2007) Paleowattmeters: a scaling relation for dynamically recrystallized grain size. Geology 35:343–346



- Azuma N, Miyakoshi T, Yokoyama S, Takata M (2012) Impeding effect of air bubbles on normal grain growth of ice. J Struct Geol 42:184–193
- Barr AC, McKinnon WB (2007) Convection in ice I shells and mantles with self-consistent grain size. J Geophys Res-Planets 112:E02012. https://doi.org/10.1029/2006JE002781
- Barr AC, Pappalardo RT (2005) Onset of convection in the icy Galilean satellites: influence of rheology. J Geophys Res-Planets 110:E12005. https://doi.org/10.1029/2004JE002371
- Barr AC, Showman AP (2009) Heat transfer in Europa's icy shell. In: Pappalardo RT, McKinnon WB, Khurana K (eds) Europa. University of Arizona Press, Tucson, AZ, USA, pp 405–430
- Bauer M, Elsaesser MS, Winkel K, Mayer E, Loerting T (2008) Compression-rate dependence of the phase transition from hexagonal ice to ice II and/or ice III. Phys Rev B 77:220105. https://doi.org/10.1103/PhysRevB.77.220105
- Baum WA, Kreidl T, Westphal JA, Danielson GE, Seidelmann PK, Pascu D, Currie DG (1981) Saturn's E ring: I. CCD observations of March 1980. Icarus 47(1):84–96
- Behn MD, Goldsby DL, Hirth G (2021) The role of grain-size evolution on the rheology of ice: implications for reconciling laboratory creep data and the Glen flow law. Cryosphere 15:4589–4605. https://doi.org/10.5194/tc-15-4589-2021
- Bennett K, Wenk HR, Durham WB, Stern LA, Kirby SH (1997) Preferred crystallographic orientation in the ice I → II transformation and the flow of ice II. Philos Mag A 76(2):413–435. https://doi.org/10.1080/01418619708209983
- Bestmann M, Pennacchioni G, Nielsen S, Göken M, de Wall H (2012)
 Deformation and ultrafine dynamic recrystallization of quartz in
 pseudotachylyte-bearing brittle faults: a matter of a few seconds.
 J Struct Geol 38:21–38. https://doi.org/10.1016/j.jsg.2011.10.001
- Billings SE, Kattenhorn SA (2005) The great thickness debate: Ice shell thickness models for Europa and comparisons with estimates based on flexure at ridges. Icarus 177(2):397–412. https://doi.org/10.1016/j.icarus.2005.03.013
- Bindschadler RA, Scambos TA (1991) Satellite-image-derived velocity field of an Antarctic ice stream. Science 252(5003):242–246
- Caswell TE, Cooper RF, Goldsby DL (2015) The constant-hardness creep compliance of polycrystalline ice. Geophys Res Lett 42(15):6261–6268. https://doi.org/10.1002/2015GL064666
- Clark RN (1981) Water frost and ice: the near-infrared spectral reflectance 0.65–2.5 μm . J Geophys Res-Solid Earth 86(B4):3087–3096
- Clark RN, Fanale FP, Zent AP (1983) Frost grain size metamorphism: implications for remote sensing of planetary surfaces. Icarus 56:233–245
- Coble RL (1963) A model for boundary diffusion controlled creep in polycrystalline materials. J Appl Phys 34(6):1679–1682
- Collins GC, McKinnon WB, Moore JM, Nimmo F, Pappalardo RT, Prockter LM, Schenk PM (2009) Tectonics of the outer planet satellites. In: Watters TR, Schultz RA (eds) Planetary tectonics. Cambridge University Press, Cambridge, pp 264–350. https:// doi.org/10.1017/CBO9780511691645.008
- Cooper RF, Kohlstedt DL (1982) Interfacial energies in the olivine basalt system. Adv Earth Planetary Sci 12:217–228
- Cooper RF, Yoon WY, Perepezko JH (1991) Internal nucleation of highly undercooled magnesium metasilicate melts. J Am Ceram Soc 74(6):1312–1319. https://doi.org/10.1111/j.1151-2916.1991. tb04104.x
- Courtney TH (1990) Mechanical behavior of materials. McGraw-Hill, New York, USA
- Cuffey KM, Thorsteinsson T, Waddington ED (2000) A renewed argument for crystal size control of ice sheet strain rates. J Geophys Res-Solid Earth 105(B12):27889–27894
- De Bresser JHP, Ter Heege JH, Spiers CJ (2001) Grain size reduction by dynamic recrystallization: can it result in major rheological

- weakening? Int J Earth Sci 90(1):28–45. https://doi.org/10. 1007/s005310000149
- Deblonde G, Peltier WR (1991) Simulations of continental ice sheet growth over the last glacial-interglacial cycle: experiments with a one-level seasonal energy balance model including realistic geography. J Geophys Res-Atmos 96(D5):9189–9215. https://doi.org/10.1029/90JD02606
- Druetta E, Nasello OB, Di Prinzio CLD (2014) Experimental determination of ⟨10-10⟩/Ψ tilt grain boundary energies in ice. J Mater Sci Res 3(1):69–76. https://doi.org/10.5539/jmsr.v3n1p
- Durham WB, Stern LA, Kirby SH (2001) Rheology of ice I at low stress and elevated confining pressure. J Geophys Res 106(6):11031-11042
- Echelmeyer KA, Harrison WD, Larsen C, Mitchell JE (1994) The role of the margins in the dynamics of an active ice stream. J Glaciol 40(136):527–538. https://doi.org/10.1017/S0022143000012417
- Evans B, Renner J, Hirth G (2001) A few remarks on the kinetics of static grain growth in rocks. Int J Earth Sci 90:88–103. https://doi.org/10.1007/s005310000150
- Exner HE (1972) Analysis of grain- and particle-size distributions in metallic materials. Int Metall Rev 17:25–42
- Fan S, Prior DJ, Cross AJ, Goldsby DL, Hager TF, Negrini M, Qi C (2021) Using grain boundary irregularity to quantify dynamic recrystallization in ice. Acta Mater 209:116810
- Feltham P (1957) Grain growth in metals. Acta Metall 5(2):97-105
- Ford HA, Fischer KM, Lekic V (2014) Localized shear in the deep lithosphere beneath the San Andreas fault system. Geology 42(4):295–298. https://doi.org/10.1130/G35128.1
- Gasson E, DeConto RM, Pollard D, Levy RH (2016) Dynamic Antarctic ice sheet during the early to mid-Miocene. Proc Natl Acad Sci USA 113(13):3459–3464. https://doi.org/10.1073/pnas.15161 30113
- Goldsby DL, Kohlstedt DL (1997) Grain boundary sliding in finegrained ice I. Scripta Mater 37(9):1399–1406
- Goldsby DL, Kohlstedt DL (2001) Superplastic deformation of ice: experimental observations. J Geophys Res-Solid Earth 106(B6):11017–11030
- Gow AJ (1969) On the rates of growth of grains and crystals in south polar firn. J Glaciol 8(53):241–252
- Herring C (1950) Diffusional viscosity of a polycrystalline solid. J Appl Phys 21:437–445
- Hillert M (1965) On the theory of normal and abnormal grain growth. Acta Metall 13(3):227–238
- Hillert M, Ågren J (2006) Extremum principles for irreversible processes. Acta Mater 54:2063–2066
- Hondoh T, Higashi A (1978) X-Ray diffraction topographic observations of the large-angle grain boundary in ice under deformation. J Glaciol 21(85):629–638
- Hoppa G, Greenberg R, Tufts BR, Geissler P, Phillips C, Milazzo M (2000) Distribution of strike-slip faults on Europa. J Geophys Res-Planets 105(E9):22617–22627
- Joughin I, Tulaczyk S, Bindschadler R, Price SF (2002) Changes in West Antarctic ice stream velocities: observation and analysis. J Geophys Res-Solid Earth 107(B11):2289. https://doi.org/10. 1029/2001JB001029
- Joughin I, MacAyeal D, Tulaczyk S (2004) Basal shear stress of the Ross ice streams from control method inversions. J Geophys Res-Solid Earth 109:B09405
- Kamb B (2001) Basal zone of the West Antarctic ice streams and its role in lubrication of their rapid motion. In: Alley RB, Bindschadler RA (eds) The West Antarctic Ice Sheet: Behavior and Environment (Antarctic Research Series Volume 77). American Geophysical Union, Washington, DC, USA, pp 157–200
- Karato S (1989) Grain growth kinetics in olivine aggregates. Tectonophysics 168:255–273



- Karato S, Wu P (1993) Rheology of the upper mantle: a synthesis. Science 260:771–778
- Karato S, Paterson MS, Fitz Gerald JD (1986) Rheology of synthetic olivine aggregates: influence of grain size and water. J Geophys Res 91(B8):8151–8176
- Kattenhorn SA, Prockter LM (2014) Evidence for subduction in the ice shell of Europa. Nat Geosci 7(10):762–767. https://doi.org/ 10.1038/ngeo2245
- Kempf S, Beckmann U, Schmidt J (2010) How the Enceladus dust plume feeds Saturn's E ring. Icarus 206(2):446–457. https://doi.org/10.1016/j.icarus.2009.09.016
- Ketcham WM, Hobbs PV (1969) An experimental determination of the surface energies of ice. Phil Mag 19:1161–1173
- Kim J-W, Ree J-H, Han R, Shimamoto T (2010) Experimental evidence for the simultaneous formation of pseudotachylyte and mylonite in the brittle regime. Geology 38(12):1143–1146
- Kingery WD, Bowen HK, Uhlmann DR (1976) Introduction to ceramics, 2nd edn. Wiley, New York, USA
- Kondepudi D, Prigogine I (1998) Modern thermodynamics: from heat engines to dissipative structures. Wiley, Chichester, England, UK
- Langdon T (1991) The physics of superplastic deformation. Mater Sci Eng, A A137:1–11
- Liu F, Baker I, Dudley M (1993) Dynamic observations of dislocation generation at grain boundaries in ice. Philos Mag A 67(5):1261–1276. https://doi.org/10.1080/01418619308224770
- McCarthy C, Cooper RF (2016) Tidal dissipation in creeping ice and the thermal evolution of Europa. Earth Planet Sci Lett 443:185–194. https://doi.org/10.1016/j.epsl.2016.03.006
- Montagnat M, Duval P (2000) Rate controlling processes in the creep of polar ice, influence of grain boundary migration associated with recrystallization. Earth Planet Sci Lett 183(1):179–186
- Mukherjee AK, Bird JE, Dorn JE (1969) Experimental correlations for high-temperature creep. Trans Am Soc Metals 62:155–179
- Nabarro FRN (1948) Deformation of crystals by the motion of single ions. In: Nooky G (ed) Report of a conference on the strength of solids. Physical Society of London, London, England, UK, pp 75–90
- Nakamura T, Matsumoto M, Yagasaki T, Tanaka H (2016) Thermodynamic stability of ice II and its hydrogen-disordered counterpart: Role of zero-point energy. J Phys Chem B 120:1843–1848. https://doi.org/10.1021/acs.jpcb.5b09544
- Newman J, Chatzaras V, Tikoff B, Wijbrans JR, Lamb WM, Drury MR (2021) Strain localization at constant strain rate and changing stress conditions: implications for plate boundary processes in the upper mantle. Minerals 11:1351. https://doi.org/10.3390/min11121351
- Nimmo F, Gaidos E (2002) Strike-slip motion and double ridge formation on Europa. J Geophys Res-Planets 107(E4):5021. https://doi.org/10.1029/2000JE001476
- Nimmo F, Giese B, Pappalardo RT (2003) Estimates of Europa's ice shell thickness from elastically-supported topography. Geophys Res Lett 30(5):1233
- Odum HT, Pinkerton RC (1955) Time's speed regulator: The optimum efficiency for maximum power output in physical and biological systems. Am Sci 43(2):331–343
- Ojakangas GW, Stevenson DJ (1989) Thermal state of an ice shell on Europa. Icarus 81(2):220–241. https://doi.org/10.1016/0019-1035(89)90052-3
- Onsager L (1931) Reciprocal relations in irreversible processes. I. Phys Rev 37:405–426
- Pappalardo RT, Head JW III, Greeley R, Sullivan RJ, Pilcher C, Schubert G, Moore WB, Carr MH, Moore JM, Belton MJS, Goldsby

- DL (1998) Geological evidence for solid-state convection in Europa's ice shell. Nature 391:365–367
- Perol T, Rice JR (2015) Shear heating and weakening of the margins of West Antarctic ice streams. Geophys Res Lett 42(9):3406–3413. https://doi.org/10.1002/2015GL063638
- Pettit EC, Waddington ED, Harrison WD, Thorsteinsson T, Elsberg D, Morack J, Zumberge MA (2011) The crossover stress, anisotropy and the ice flow law at Siple Dome, West Antarctica. J Glaciol 57:39–52
- Poirier J-P (1985) Creep of crystals. Cambridge University Press, Cambridge
- Pollard D, DeConto RM (2009) Modeling West Antarctic ice sheet growth and collapse through the past five million years. Nature 458:329–332. https://doi.org/10.1038/nature07809
- Porco CC, Helfenstein P, Thomas PC, Ingersoll AP, Wisdom J, West R, Neukum G, Denk T, Wagner R, Roatsch T, Kieffer S, Turtle E, McEwen A, Johnson TV, Rathbun J, Veverka J, Wilson D, Perry J, Spitale J et al (2006) Cassini observes the active south pole of Enceladus. Science 311:1393–1401
- Porco C, DiNino D, Nimmo F (2014) How the geysers, tidal stresses, and thermal emission across the south polar terrain of Enceladus are related. Astron J 148(3):45. https://doi.org/10.1088/0004-6256/148/3/45
- Prigogine I (1997) The end of certainty: time, chaos, and the new laws of nature. The Free Press, NewYork, USA
- Prior DJ, Lilly K, Seidemann M, Vaughan M, Becroft L, Easingwood R, Diebold S, Obbard R, Daghlian C, Baker I, Caswell T, Golding N, Goldsby D, Durham WB, Piazolo S, Wilson CJL (2015) Making EBSD on water ice routine. J Microsc 259(3):237–256. https://doi.org/10.1111/jmi.12258
- Raj R (1975) Transient behavior of diffusion-induced creep and creep rupture. Metall Trans A 6A:1499–1590
- Raj R (1981) Morphology and stability of the glass phase in glassceramic systems. J Am Ceram Soc 64(5):245–248
- Raj R, Ashby MF (1971) On grain boundary sliding and diffusional creep. Metall Trans 2:1113–1127
- Ranganathan M, Minchew B, Meyer CR, Peč M (2021) Recrystallization of ice enhances the creep and vulnerability to fracture of ice shelves. Earth Planet Sci Lett 576:11721. https://doi.org/10.1016/j.epsl.2021.117219
- Rozel A, Ricard Y, Bercovici D (2011) A thermodynamically self-consistent damage equation for grain size evolution during dynamic recrystallization. Geophys J Int 184:719–728. https://doi.org/10.1111/j.1365-246X.2010.04875.x
- Rutter EH, Brodie KH (1988) The role of tectonic grain size reduction in the rheological stratification of the lithosphere. Int J Earth Sci 77(1):295–307
- Schmalzried H (1995) Chemical kinetics of solids. VCH Publishers, Weinheim, FRG
- Schoof C (2010) Ice-sheet acceleration driven by melt supply variability. Nature 468:803–806. https://doi.org/10.1038/nature09618
- Sejrup HP, Clark CD, Hjelstuen BO (2016) Rapid ice sheet retreat triggered by ice stream debuttressing: evidence from the North Sea. Geology 44(5):355–358. https://doi.org/10.1130/G37652.1
- Shimizu I (1998) Stress and temperature dependence of recrystallized grain size: a subgrain misorientation model. Geophys Res Lett 25(22):4237–4240
- Smith SAF, Di Toro G, Kim S, Ree J-H, Nielsen S, Billi A, Spiess R (2013) Coseismic recrystallization during shallow earthquake slip. Geology 41(1):63–66. https://doi.org/10.1130/G33588.1
- Spahn F, Schmidt J, Albers N, Hörning M, Makuch M, Seiß M, Kempf S, Srama R, Dikarev V, Helfert S, Moragas-Klostermeyer G, Krivov AV, Sremčević M, Tuzzolino AJ, Economou T, Grün E (2006) Cassini dust measurements at Enceladus and implications for the origin of the E ring. Science 311:1416–1418



- Speciale PA, Behr WM, Hirth G, Tokle L (2020) Rates of olivine grain growth during dynamic recrystallization and postdeformation annealing. J Geophys Res-Solid Earth 125:e2020JB020415. https://doi.org/10.1029/2020JB020415
- Stern LA, Durham WB, Kirby SH (1997) Grain-size-induced weakening of H₂O ices I and II and associated anisotropic recrystallization. J Geophys Res-Solid Earth 102(B3):5313-5325. https://doi. org/10.1029/96JB03894
- Suckale J, Platt JD, Perol T, Rice JR (2014) Deformation-induced melting in the margins of the West Antarctic ice streams. J Geophys Res-Earth Surf 119(5):1004-1025. https://doi.org/10.1002/2013J F003008
- Sutton AP, Balluffi RW (1995) Interfaces in crystalline materials. Clarendon Press, Oxford
- Tobie G, Choblet G, Sotin C (2003) Tidally heated convection: constraints on Europa's ice shell thickness. J Geophys Res-Planets 108(E11):5124. https://doi.org/10.1029/2003JE002099
- Tufts BR, Greenberg R, Hoppa G, Geissler P (1999) Astypalaea Linea: a large-scale strike-slip fault on Europa. Icarus 141:53-64
- Tulaczyk S, Kamb B, Engelhardt HF (2001) Estimates of effective stress beneath a modern West Antarctic ice stream from till preconsolidation and void ratio. Boreas 30(2):101-114
- Twiss RJ (1977) Theory and applicability of a recrystallized grain size paleopiezometer. Pure Appl Geophys 115:227-244

- Verberne BA, Plümper O, de Winter DM, Spiers CJ (2014) Superplastic nanofibrous slip zones control seismogenic fault friction. Science 346(6215):1342-1344
- Walpole RE, Myers RH (1972) Probability and statistics for engineers and scientists. Macmillan Co, New York
- Warren JM, Hirth G (2006) Grain size sensitive deformation mechanisms in naturally deformed peridotites. Earth Planet Sci Lett 248:438-450
- Whillans IM, van der Veen CJ (1997) The role of lateral drag in the dynamics of Ice Stream B. Antarctica. J Glaciol 43(144):231-237
- Willis JK, Church JA (2012) Regional sea-level projection. Science 336:550-551
- Ziegler H (1958) An attempt to generalize Onsager's principle, and its significance for rheological problems. Z Angew Math Phys 9b:748-763
- Ziegler H, Wehrli C (1987) The derivation of constitutive relations from the free energy and the dissipation function. Adv Appl Mech 25:183-238

Publisher's Note Springer Nature remains neutral with regard to jurisdictional claims in published maps and institutional affiliations.

